STUDIA UBB CHEMIA, LXX, 3, 2025 (p. 35-53)
(RECOMMENDED CITATION)
DOI:10.24193/subbchem.2025.3.03

PHYSICOCHEMICAL INVESTIGATION OF SOME GEOTHERMAL WATERS FROM SALAJ COUNTY ROMANIA

Simona Elena AVRAM[a], Cristian MANDIUC[a], Ioan PETEAN[b,*], Lucian Barbu TUDORAN[c,d], Gheorghe BORODI[d,*]

ABSTRACT. Geothermal waters solve minerals from the geological layers due to their increased temperature. These minerals affect water hardness and salinity. Therefore, thermal water samples were collected from spa pools springs in Salaj County Romania: Broscarie (Simleul Silvaniei), Jibou, and Boghis. The physicochemical measurement reveal that Jibou water has higher electrical conductivity of 10580 µSi/cm caused by the higher value of total dissolved solids (TDS) of 5264 mg/l, it is followed by Broscarie water having an electrical conductivity of 1949 µSi/cm related to TDS of 1023 mg/l. The weaker mineralization was found in Boghis water around of 619 mg/l corresponding to an electrical conductivity of 1200 µSi/cm. Water hardness is related to $CaCO_3$ amount. Boghis water is the harder containing 356 mg/l followed by Broscarie having 178 mg/l. Jibou water is the softer having $CaCO_3$ about 106.8 mg/l. The mineral distribution was assessed by mineralogical optical microscopy (MOM) and X ray diffraction (XRD). It results that NaCl crystallized as halite is responsible for the samples salinity while aragonite, magnesian calcite and calcite are the minerals which causes the water hardness. Hard thermal water containing Ca and Mg are effective for rheumatoid symptoms amelioration while salted water is optimal for skin care.

Keywords: *Thermal water, mineral content, hardness, salinity.*

[a] *Faculty of Materials and Environmental Engineering, Technical University of Cluj-Napoca, 103-105 Muncii Bd., RO-400641, Cluj-Napoca, Romania.*
[b] *Faculty of Chemistry and Chemical Engineering, Babes-Bolyai University, 11 Arany Janos Street, 400028 Cluj-Napoca, Romania.*
[c] *Faculty of Biology and Geology, Babes-Bolyai University, 44 Gheorghe Bilaşcu Street, 400015 Cluj-Napoca, Romania.*
[d] *National Institute for Research and Development of Isotopic and Molecular Technologies, 65-103 Donath Street, 400293 Cluj-Napoca, Romania.*
[*] *Correspondent authors:* ioan.petean@ubbcluj.ro*;* borodi@itim-cj.ro

©2025 STUDIA UBB CHEMIA. Published by Babeş-Bolyai University.

This work is licensed under a Creative Commons Attribution-NonCommercial-NoDerivatives 4.0 International License.

INTRODUCTION

Geothermal waters are formed into the deeper geological formation heated by the magma layer. They are most likely occur through the tectonic faults which facilitates the water infiltration and it's subsequently lift as hot springs [1, 2]. The increased temperature facilitates minerals dissolution enriching water is specific ions depending on the geological layers composition [3]. The dominant mineral imposes the geothermal characteristic as: carbonated when CO_2 interacts with Ca and Mg from sedimentary rocks, sulphurated geothermal water contains S from the rocks interaction with H_2S or from biogenic sources like sulfur bacteria [4, 5]. On the other hand, salted water are formed by the water interaction with Halite evaporite deposits (NaCl crystallized in cubic system), without need of thermal energy [6, 7]. High temperature of the geothermal water increases the Halite solubility in water and therefore it is often found in geothermal and mineral waters in various ratios depending on its occurrence on the geological layers.

Salaj County is situated in northwestern side of Romania and is affected by the North Transylvanian fault influencing the sedimentary layers [8]. For instance, Simleul Silvaniei is influenced by the Badenian deposits including yellow sand, crystalline conglomerates, sandstone and evaporite deposits. Krezsek and Bally reports sedimentary layers of sandstone, limestone with crystalline conglomerates formed in Eocene period [8]. Thus, Jibou Formations includes Lower Variegated Red Shales and Rona limestone interfered with some evaporitic salt deposits [9, 10]. Similar sedimentary conditions are reported in literature for Boghis area influencing the geothermal water mineral content [11]. The local tectonic rift and the geological layers interaction with water deposits facilitate its emergence to the surface as hot geothermal springs in Simleul Silvaniei, Jibou and Boghis. These springs were collected directly from the source and the water is currently used for spa pools.

Sandstone is a pressed conglomerate formed by quartz sand and clay fine fractions as granular filler and calcium carbonate as mineral binder. This binder most likely occurs as calcite crystallized in Trigonal system and less crystallized in orthorhombic system as aragonite as occurs in limestone [12, 13]. Calcium carbonate has a limited solubility in water of about 13 mg/l at 25 °C and increases with temperature, therefore the geothermal water are enriched in Ca^{2+} ions [13].

Sandstone and limestone might contain $CaMg(CO_3)_2$ crystallized in Trigonal system having ordered successive layers of Mg and Ca atoms and consist in a major source of magnesium within geothermal water [14]. The other source of magnesium within the geothermal water is magnesian clays mineral such as palygorskite, sepiolite and kerolite but it might occurs as

impurities in red clays like Muscovite and Biotite replacing some of the Fe atoms in their structure. Water, especially at high temperature, penetrates the clay interplanar layers solving some of their mineral content [15, 16].

Badenian evaporite deposits within the Transylvanian Basin are formed mainly by NaCl crystallized in cubic system as halite. However they might be accompanied by moderate amounts of calcium sulfate crystallized as gypsum or anhydrite [17, 18]. Halite has an extremely high solubility in water around of 360 g/L at 25 °C, compared to calcite and dolomite and strongly increases with the temperature [19]. Thus, the evaporitic deposits are quickly dissolved by the hot water while carbonaceous rocks take longer. Larger geothermal water deposits have long interaction with the geological layers until burst out from the ground as hot springs collecting the specific mineral amount. A complete investigation regarding their mineralization mechanism would require detailed geological drillings for accurate establishing of each stone layer's composition. Hence, the geological drillings are very expensive and require a lot of work on the field, relevant information regarding the water mineralization can be obtained through their in vitro crystallization.

One of our previous studies reveals successfully the mineralization within the public springs in Borsec [20]. Water physicochemical properties like pH, turbidity, of total dissolved solids (TDS), salinity, electrical conductivity and chloride content were correlated with the specific mineral crystallization. These aspects were reveled with some targeted investigation: minerals formation and crystallization was investigated by X-ray diffraction (XRD) coupled with optical mineralogical microscopy (MOM), morphological aspects were correlated with the elemental composition through the SEM – EDX analysis. It was found that pre-existent solid particles dispersed in the water samples (samples with high turbidity) acts as germination seeds while in the clear water samples crystallization germs precipitates through the homogeneous germination under concentration gradient induced by the water evaporation. Such behavior was also reported in literature for the Pharmacolite ($CaHAsO_4 \cdot 2H_2O$) along with carbonates [21]. It is expected that a competitive behavior will occur between the crystallization of carbonates and halides when the collected water samples are dried.

The aim of present research is to discover a sustainable approach of these geothermal waters based on their physicochemical properties correlation with the crystallization of mineral content during the natural drying.

RESULTS AND DISCUSSION

The mineral charge has a strong influence on the physicochemical characteristics of the water samples. It results that all investigated springs have slightly alkaline pH around 8, Figure 1a, forming a single relevant statistical group.

It indicates a balance between carbonated and salted mineralization which is proper for curative baths. The constant ph values for the waters collected from all 3 investigated sites rely on the similar sedimentary geological formations interacting with hot water.

Turbidity represents another general physical characteristic of the water samples revealing the presence or absence of the solid particles dispersed within. Figure 1b reveal that samples from Broscarie and Boghis are clear having turbidity below the detection limit and thus forms a relevant statistical group. It might be a characteristic favored by their temperature of about 40 ˚C at collection moment. Water samples collected from Jibou has a turbidity of about 6 FTU which is a low value according to the Directive (EU) 2020/2184. However the statistical analysis indicates that Jibou sample forms the second statistical relevant group. Statistical comparing of these two groups reveals statistical differences $p < 0.05$. It might influence the crystallization process through the solid dispersoids acting as heterogeneous crystallization germs.

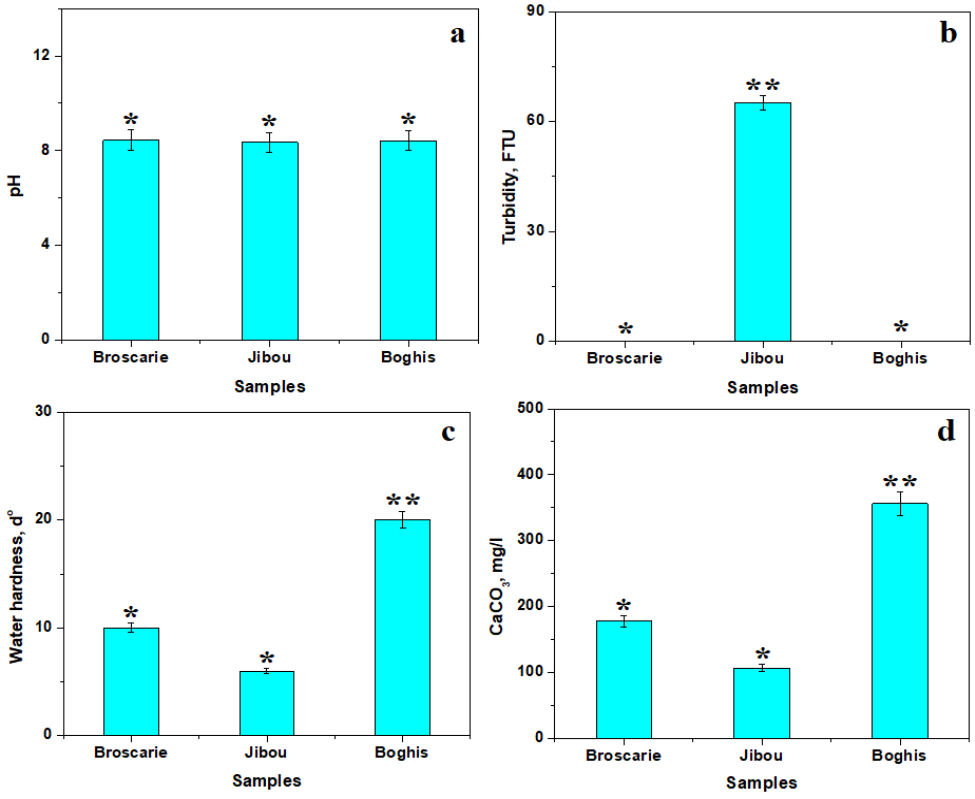

Figure 1. General physicochemical parameters of the water samples: a) pH, b) Turbidity, c) Hardness and d) $CaCO_3$ amount.

Water hardness is a measure of the carbonate mineralization which are dissolved from the sedimentary deposits, Figure 1c. The samples collected from Broscarie and Jibou have hardness below 10 dH˚ indicating a moderate carbonation, therefore forms a relevant statistical group. Boghis water has almost double hardness indicating a more carbonated nature, thus it forms the second relevant statistical group. There are statistical differences between the observed groups. Calcium carbonate amount was determined based on the hardness results, Figure 1d. It results that Broscarie water has calcium carbonate about of 178 mg/l followed by Jibou sample with 106.8 mg/l. The water sample collected from Boghis has a more enhanced carbonated characteristic having dissolved $CaCO_3$ about of 356 mg/l. These values are very important for understanding the crystallization process.

Total dissolved solids (TDS) comprises both dissolved carbonates but are prone affected by the halite dissolution as observed in literature [6, 7]. Figure 2a reveal that Broscarie and Boghis samples have relatively low TDS below 2000 mg/l forming a relevant statistical group totally different regarding Jibou sample having high TDS value of about 5000 mg/l. TDS also influences the electrical conduction by providing mobile ions ensuring the electrical charge movement thus the water samples collected from Broscarie and Boghis have moderate electrical conductivity while Jibou water has a high electrical conductivity. It certainly prove the statistical difference between observed groups $p < 0.05$, Figure 2b.

Salinity represents a specific measure of the dissolved sodium chloride, Figure 2c, and strongly relates with the values of the total Cl, Figure 2d. Thus, sample collected from Broscarie has a salinity of 1.17 PSU which agrees the total Cl of 0.15 mg/l while Boghis water has a lower salinity of only 0.69 PSU related to slightly lower amount of total Cl of about 0.1 mg/l. On the other hand, Jibou sample has increased salinity of about 6.7 PSU which is confirmed by high amount of total Cl which is about 3.5 mg/l. The statistical analysis indicates that Broscarie and Boghis waters are less salted than Jibou water and the salty behavior is given by the dissolved halite.

TDS values variation indicates a strong mineralization within the investigated samples which should promote a particularized crystallization of each sample. The long time crystallization process developed in Petri dishes is developed by the progressive evaporation of the water inducing a concentration gradient that facilitate crystals formation and their subsequently growth. The mineral crusts formed in the Petri dishes were optically inspected in reflected light, Figure 1.

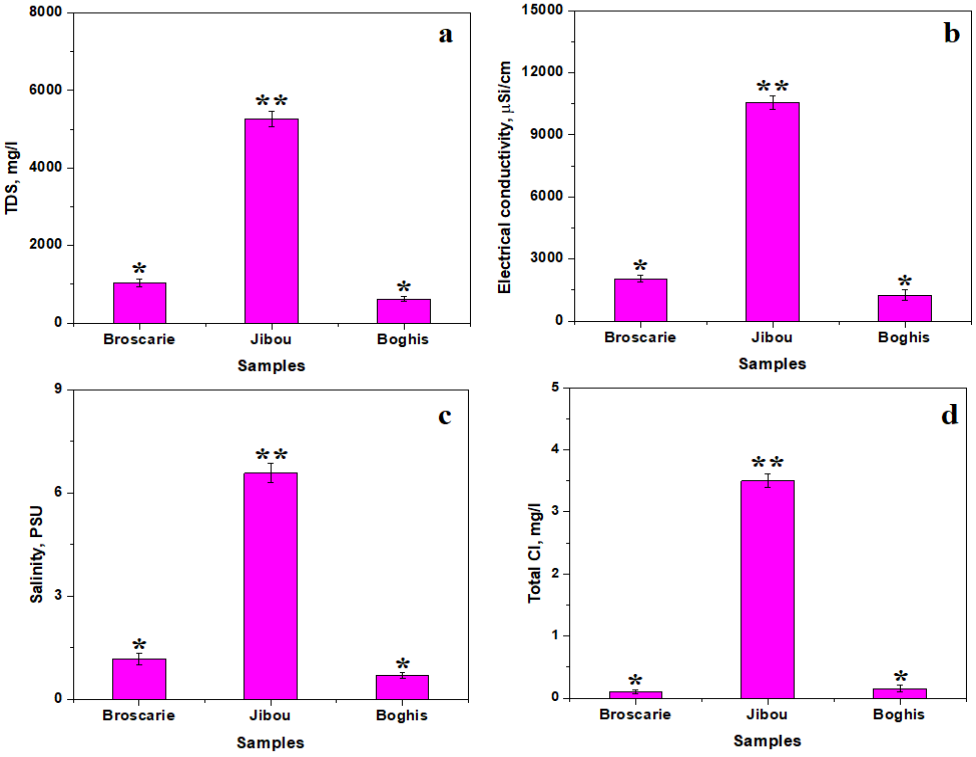

Figure 2. Specific physicochemical parameters of the water samples:
a) TDS, b) Electrical conductivity, c) Salinity and d) Total Cl.

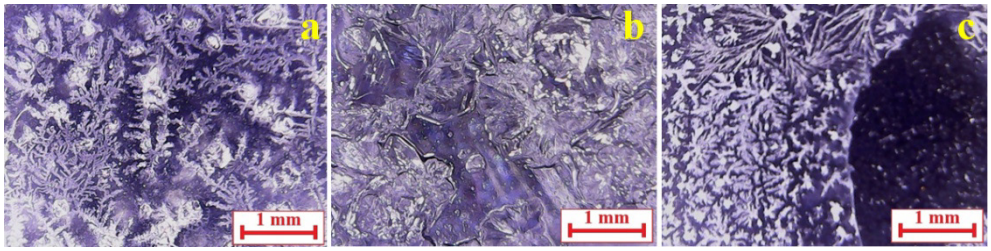

Figure 3. Optical microstructure observed in reflected light:
a) Broscarie, b) Jibou, and c) Boghis.

Sample collected from Broscarie has a moderate mineralization directly related to the TDS amount and reveal relatively equiaxed crystal clusters ranging from about 300 – 800 µm in diameter most likely belonging to the calcium carbonate formation, Figure 3a. These are surrounded in a dense manner by the NaCl dendrites.

The sample collected from Jibou has a high salinity and moderate carbonate content, fact influencing the microstructural aspect of the crystallized crust, Figure 3b. It has well defined carbonate clusters disposed in local nests with diameters ranging from 500 to 900 μm interlaced with large cubic crystals of NaCl and a dense structure of fine dendrites.

Physicochemical measurements reveal that Boghis sample has an increased hardness and lower salinity indicating that carbonates are the main crystalline components in the formed crust, Figure 3c. There is fine carbonate clusters promoting a branched structure imitating bushes embedded in a tiny mineral crust which might be related with the lower amounts of NaCl. The general optical inspection is not sufficient for a proper assessment of the crystallization process. Therefore the mineral crusts formed in the Petri dishes were subjected to the optical mineralogical microscopy and afterwards erased and transformed in powder which was subjected to the X ray diffraction (XRD) resulting the patterns presented in Figure 3.

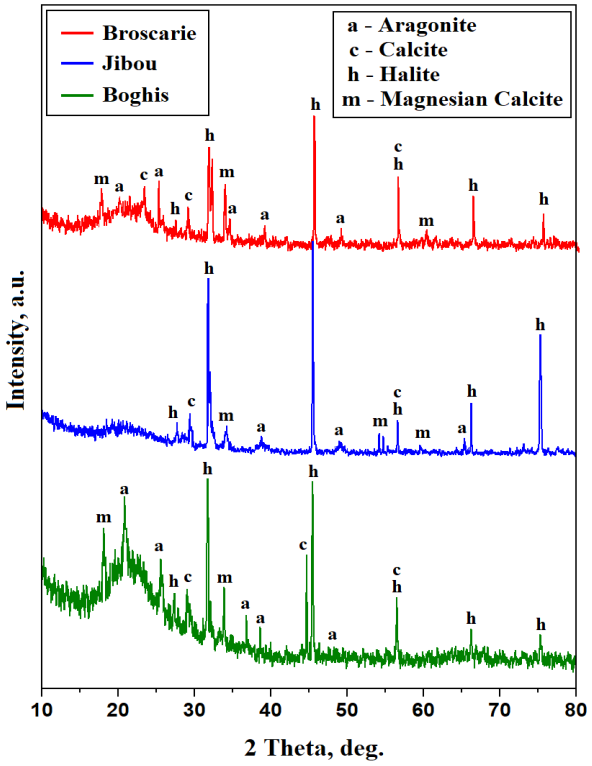

Figure 4. The XRD patterns for the crystallized minerals: aragonite PDF 71-2396; calcite PDF 86-2339; halite 77-2064; magnesian calcite PDF 89-1305.

The XRD patterns in figure 4 are well developed having narrow aspect and strong intensities corresponding to the high degree of crystallinity of the investigated powders. NaCl crystallized as halite has a very ordered crystal structure within face centered cubic system (FCC) having alternant atoms of Na and Cl centering each other cubic faces [22]. Therefore it exhibits more intense peaks regarding Trigonal and orthorhombic crystals of carbonate minerals. This difference is quantified by the Corundum Factor. Thus, apparently Halite dominates all samples but we observe strong and well developed peaks for carbonate minerals such Aragonite, Calcite and magnesian calcite in samples from Boghis and Broscarie. Each mineral amount can be calculated using the Relative Intensity Ratio (RIR) method previously described in literature [23, 24]. The obtained amounts are centralized in Table 1.

Table 1. Samples mineral characteristics revealed by XRD and MOM

Component	**Aragonite**	**Calcite**	**Magnesian Calcite**	**Halite**
Formula	$CaCO_3$	$CaCO_3$	$CaMg(CO_3)2$	NaCl
Crystal system	Orthorombic	Trigonal	Trigonal	Cubic
Color in cross polarized light	blue-violet	white -brown	white - yellow	transparent pale blue
Particle shape	rhombic	pseudo hexagonal	columnar	cubic rectangular
Broscarie				
Amount, wt.%	22	13	37	28
Particle size range, μm	200 - 400	50 - 150	200 - 600	10 - 200
Jibou				
Amount, wt.%	8	14	26	52
Particle size range, μm	50 - 150	50 - 600	200 - 600	10 - 300
Boghis				
Amount, wt.%	19	28	35	18
Particle size range, μm	100 - 250	50 - 600	200 - 800	-

The crystals size ranges were measured after the long time crystallization in Petri dishes.

It results that sample collected from Broscarie is dominated by the magnesian calcite and followed by halite. Significant amounts of aragonite were found and only moderate amounts of pure calcite. Jibou sample is clearly dominated by halite amounts followed by carbonated minerals. Magnesian Calcite is the most representative carbonated mineral followed by the pure Calcite wile Aragonite occurs almost as traces. On the other hand, Boghis sample is completely dominated by the carbonated minerals such as: magnesian calcite, pure calcite and aragonite and only small amounts of Halite were found.

XRD allow the proper identification of the crystallized minerals and their amounts but lacks in evidencing their distribution which should be followed under cross polarized light inspection through the mineralogical microscopy. The literature data reveal that aragonite specific colors ranges from blue to violet depending on the crystal position regarding the microscope optical axis. Magnesian calcite has predominantly pale yellow color while pure calcite is prone white. Halite crystals are mostly transparent and therefore it features a pale blue hue at the contact interface with other developed minerals [20, 22]. Thus, MOM investigation has the benefit of observing the crystallization process directly on the glass slide revealing the incipient crystals evolution up to the complete evaporation of the water.

Broscarie water has turbidity below detecting limit proving that there are no solid dispersed particles to facilitate crystals precipitation. Water evaporation induces a concentration gradient. The first germination seeds start precipitating when the liquid sample reaches the calcium carbonate supersaturating limit of 13 mg/l. In consequence, we found calcite crystallization centers having pseudo-hexagonal shapes and sizes of 10 – 15 μm appearing as small white spots randomly dispersed on the observation field within Figure 5a. The magnesian calcite forms columnar crystals of about 25 – 50 μm in length and about 5 μm widths disposed radially around the germination seed. The sodium chloride is still solved into the remnant liquid. The final stage of crystallization on the glass slide occurs after 24 hours after the drops deposition. The precipitated calcite has almost no changes in shape, size and distribution but magnesian calcite crystals strongly increases to about 300 μm in length keeping their radial disposal, Figure 5b. All carbonate crystal is surrounded by fine network of halite dendrites having pale blue nuance, but these are less visible due to the relative quick crystallization on the glass lamella. The long time crystallization (about 1 week) takes place in to the Petri dish. All crystals are better grown having bigger sizes and are better represented including the halite dendrites, Figure 5c.

Several microstructural details were taken on the best specimens of each crystals formed by drying of Broscarie water. Thus, Figure 5d reveal two aragonite clusters having rhombic crystals ranging from 50 to 100 μm associated each other resembling butterflies, the specific blue – violet color is better observed on their sides. The best specimen of magnesian calcite is observed in Figure 5e where 6 crystals grow radially around the germination seed having different lengths (shorter on the base having length of 150 μm and longer on the top having about 650 μm) displaying a flowery look. Halite dendrites are better observed in Figure 5f having a squared stem and lateral branched formed by small cubic crystals. The dendrite length is longer than 800 μm. Some pseudo-hexagonal calcite crystals having white appearance can be observed in the right lower side of Figure 5f.

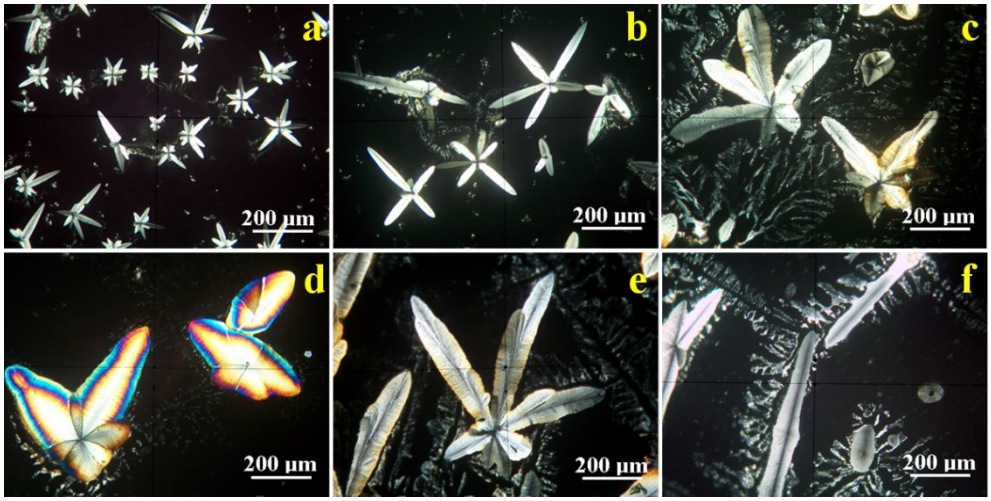

Figure 5. Crystals development in Broscarie sample observed by mineralogical optical microscopy: a) initial crystallization stage on glass slide, b) final crystallization stage on glass slide, c) long time crystallization in Petri dish. Microstructural details on specific crystals: d) aragonite, e) magnesium calcite and f) halite dendrites embedding calcite.

Jibou water very salty of about 6.7 PSU but also has a significant turbidity about 6 FTU indicating the presence of solid particles dispersed within. Several small yellow dots are observed floating in the liquid during the initial stage of crystallization, Figure 6a. These have strong resemblance to sulfur according to the literature [25] and most likely occur as organo-synthesis made by the sulfur bacteria [26]. These small dots act as heterogeneous crystallization germs facilitating appearance of small magnesian calcite radial clusters and some white pseudo – hexagonal Calcite particles. It fits the usual crystallization pattern but the most notable difference is the occurrence of well defined halite crystals beginning to form dendrites.

The end stage of crystallization on the glass slide, Figure 6b, reveal the carbonate crystals overwhelmed by the halite formation with two strong dendrites having over 800 µm length and lateral branches of about 100 – 150 µm. The inter-dendritic spaces also contain well developed halite crystals growth on [100] and [110] directions having cubic or rectangular shape. The long term crystallization in Petri dish allow a regrouping of the carbonate crystals into some “composite leaf” with the base attached onto central large square pyramidal halite crystal growth on the [220] with octahedral resemblance. Leafs looks palmate and contains a mixture of magnesian calcite, aragonite and

calcite, Figure 6c. Specific details found on some of leafs gathering into their structure only Calcite crystals, Figure 6d and magnesian calcite in Figure 6e. These formations are surrounded by the halite dendrites. Figure 6f reveal an interesting morphology centered on two Aragonite crystals having rhombic aspect and specific blue – violet nuance. These are partly covered by a dense cloud of fine yellow particles which resemble to the sulfur clusters.

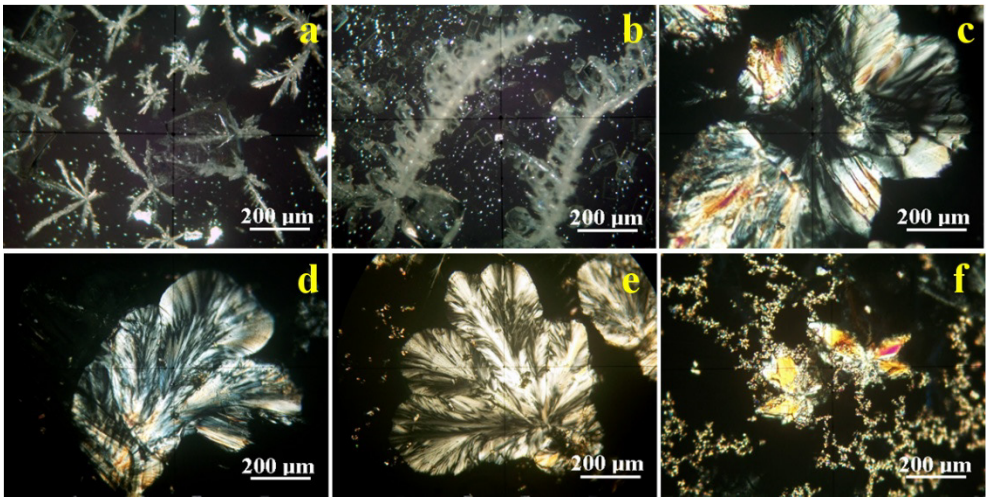

Figure 6. Crystals development in Jibou sample observed by mineralogical optical microscopy: a) initial crystallization stage on glass slide, b) final crystallization stage on glass slide, c) long time crystallization in Petri dish. Microstructural details on specific crystals: d) calcite surrounded by halite dendrites, e) magnesium calcite and f) aragonite surrounded by small S clusters.

The mineral amount within Boghis water is lower than in the other investigated samples having TDS only 619 mg/l correlated with relatively high hardness characteristic indicate a strong carbonated behavior. Therefore, the initial stage of crystallization is dominated by formation of radial clusters of mixed magnesian calcite and calcite while aragonite is less observed, Figure 7a.

The radial clusters progressively grow and reorganize their positions forming calcified branches consolidated by the precipitation of newest formed crystallites until the final stage of crystallization on the glass slide, Figure 7b. Their length is greater than 2 µm but they are still thin because of the shorter crystallization time (10 – 35 µm). The lower amount of chlorine within Boghis water reduces considerably the halite amount which forms thin crusts between the calcified branches inducing a blue hue over their sides.

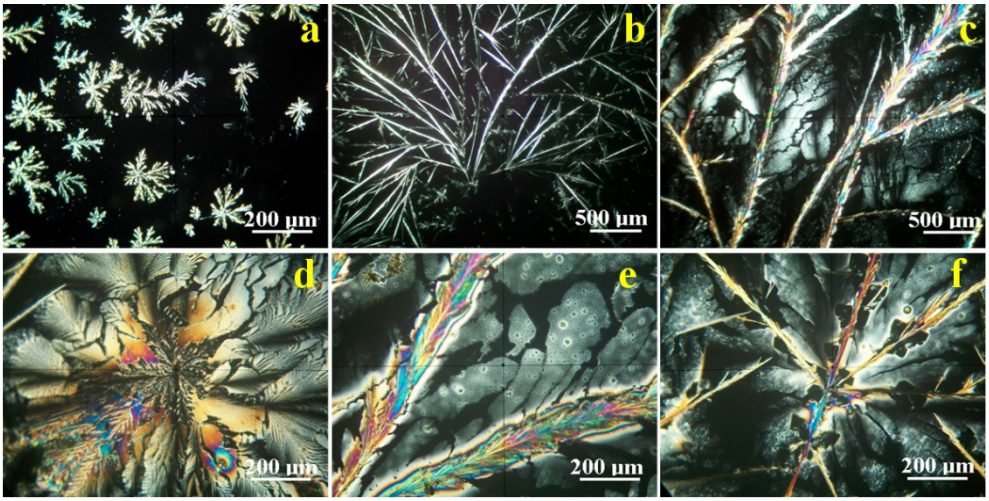

Figure 7. Crystals development in Boghis sample observed by mineralogical optical microscopy: a) initial crystallization stage on glass slide, b) final crystallization stage on glass slide, c) long time crystallization in Petri dish. Microstructural details on specific crystals: d) aragonite and magnesium calcite, e, f) Calcified branches surrounded by halite crusts.

The long term crystallization allow a massive regrouping of the carbonate crystals in more developed branches as observed in Figure 7c. Their length seems to be the same but the thickness increases to about 50 – 200 µm depending on their position regarding the initial crystallization center. The halite crusts are more evident having pale blue nuance filling inter-dendritic space. Microstructural detail in Figure 7d reveals a radial distribution of the carbonate minerals around a crystallization center. The inner area is characterized by the predominantly yellow white nuance characteristic for magnesian calcite with small iridescent aragonite crystallite. The outer area of the formation contains predominantly calcite crystallites grouped in compact areas. On the other hand, the microstructural aspect of the branches derived from the central formations, Figure 7e reveal a complex mixture of magnesian calcite, calcite and aragonite while halite crusts fill the adjacent space, Figures 7e and f.

The crystallization experiments reveal that the sodium chloride amount within the water samples play a key role in the shape and size of the calcium carbonate crystals size and shape. Higher NaCl concentration (Jibou sample) lead to large formations of the carbonate crystals individualized or mixed in complex structure resembling to leaf aspect. Moderate amount of sodium chloride as observed in Broscarie water ensure a coherent deposition of the

newly precipitate crystalline matter over the formed crystals facilitating their size growth. It looks that lower sodium chloride amount facilitates the branch crystallization through the concentration gradient during the slow drying in the Petri dish.

The powder examined by XRD was subjected to SEM investigation and the elemental distribution was revealed, Figure 8. The broken crystals within Broscarie sample reveal pseudo-hexagonal and rhombic particles colored in light green nuance due to the yellow label assigned to C, green label assigned to Ca and light blue assigned to O. Their size ranges from 5 to 10 μm in good agreement with MOM observation. The central side of Figure 8a reveal a Magnesian Calcite fragment broken from a large acicular crystal, its specific footprint is given by the pink spots over its green surface indicating the random presence of Mg atoms within $CaMg(CO_3)_2$ structure. The halite crust traces are revealed by local violet hue associated with Na atoms.

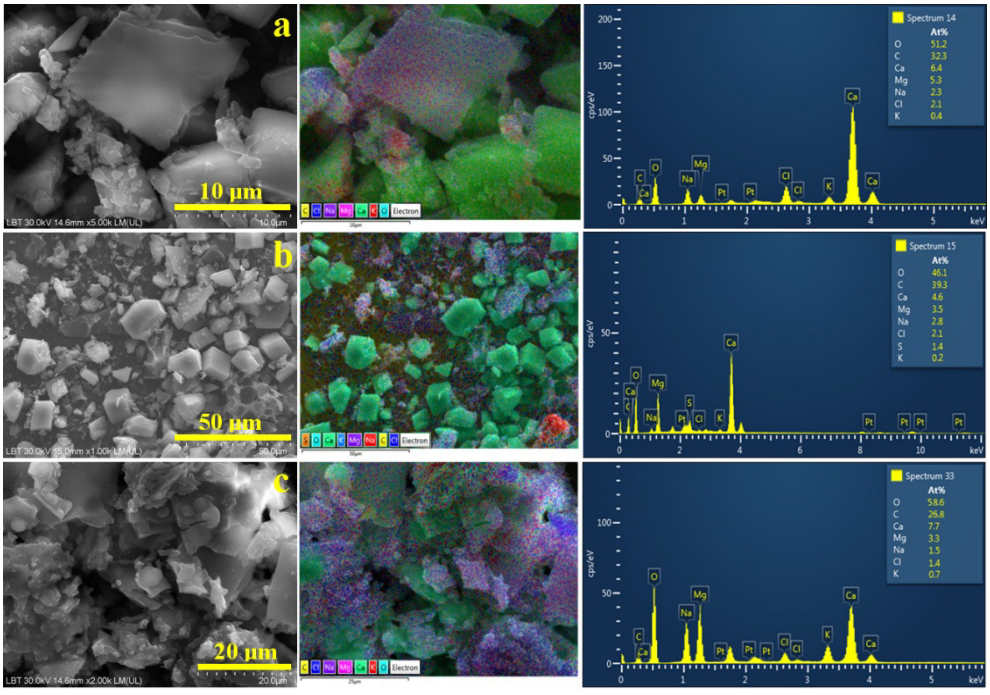

Figure 8. SEM secondary electron images (SEI) of the mineral powder crystallized from the water samples: a) Broscarie, b) Jibou, and c) Boghis. The equivalent backscattered electron image featuring elemental distribution map and the EDS spectrum are presented in the right side of each SEI image.

Jibou powder sample reveals broken pseudo-hexagonal calcite and rhombic aragonite crystals along with fine sand resulted from the broken magnesian calcite crystals. The large amount of crystallized NaCl generates well individualized Halite particles having red appearance because of red label of Na atoms (the lower right side of Figure 8b).

Boghis water, Figure 8c, looks rich in Magnesian Calcite particles mixed up with Calcite and Aragonite broken crystals. There are mostly finest particles below 5 μm resulted from the broken calcified branches. Na distribution is poorly observed only as marginal deposits because of low Halite content of the sample. The elemental composition of the mineral powder crystallized from the water samples is centralized in Table 2.

Table 2. Crystal powder elemental composition

Element	Elemental composition, at.%							
	O	C	Ca	Mg	Na	Cl	K	S
Broscarie	51.2	32.3	6.4	5.3	2.3	2.1	0.4	-
Jibou	46.1	39.3	4.6	3.5	2.8	2.1	0.2	1.4
Boghis	58.6	26.8	7.7	3.3	1.5	1.4	0.7	-

The elemental composition is dominated by O and C in all samples proving their rich carbonaceous nature. Boghis water is richest in Ca while Jibou sample has the lower amount, fact in good agreement with water hardness measurements. Na and Cl amounts are almost identical in Broscarie and Jibou samples while Boghis sample has lower values proving its low salinity. Sulfur was not detected in Broscarie and Boghis water but we found significant amount of 1.4 at.% in Jibou water confirming that the small yellow dots observed by mineralogical optical microscopy in Figure 6f are indeed sulfur clusters.

The elevated temperature of about 40 °C within Broscarie and Boghis water combined with their significant content in Ca^{2+} and Mg^{2+} ions prove to be effective for amelioration of rheumatic symptoms because of their anti-inflammatory effect. For instance, Verhagen et.al evidence the pain relief induced by Ca^{2+} and Mg^{2+} ions during the balneotherapy cures mainly due to the physicochemical effects on the inflamed areas because of their penetration through skin which avoid dietary metabolic flow [27]. The benefit of carbonaceous geothermal waters on rheumatic affection alleviation is also confirmed by Romay-Barrero indicating a Ca content of 432.7 mg/l and Mg of about 88.5 mg/l related to a HCO_3^- of 109.8 mg/l [28]. It clearly indicate that Boghis water perfectly fits the requirements for alleviating rheumatic symptoms followed closely by Broscarie water which is slightly less mineralized with Ca and Mg.

Saline and sulfur geothermal water are renowned for skin care treatments since antiquity their efficacy being reported for various skin diseases such as dermatitis and moderate fungal infections but also alleviate symptoms regarding psoriasis and atopic dermatitis [29, 30]. Jibou water best fits this application field because of the high salinity and the other proactive minerals, and is closely followed by Broscarie water which has significant salinity beside its carbonated characteristic. The significant amount of sulfur detected in Jibou water makes it proactive for treatment of moderate fungal infections beside its tendency to forms scales deposits on the spa installation pipes because facilitation of carbonate mineral precipitation as observed in our sample by MOM microscopy [31].

Literature data reports the successfully mixing of such geothermal waters with peloid particles like clays [32, 33]. On the other hand natural peloids (medicinal muds) containing geothermal water and clay soil particles were tested for potential toxicological effects against white mustard and Eisenia worms. It was found that targeted peloids have no acute toxicity but reduces the growth of Eisenia worms while white mustard remains unaffected [34]. Volcanic associated geothermal systems combined with local clays generate sulfur based peloid like the unique one formed Copahue volcano in Argentina [35]. The peloid is based mainly on beidelite and kaolinite mixed up with solute ions of $S0_4^{2-}$ and S^{2-} becoming so called clayey–sulphurous mud having therapeutic action skin affections [35]. Thus, present article opens a research path regarding the targeted water samples. It can be the start point for more detailed investigations which allows finding of specific application in spa therapy. One of the potential direction would be the development of advanced peloid based on this geothermal waters as dispersion environment for specific sorts of clays.

CONCLUSIONS

The conducted investigations on the targeted geothermal water reveal useful conclusions regarding their physicochemical behavior. The crystal formation is strongly influenced by the samples salinity which has a strong influence on the carbonate mineral precipitation and crystal growth. The higher salinity determines coalescence of small carbonate crystals and their further fusion into larger crystals at longer evaporation times.

Magnesian calcite is the dominant carbonated mineral followed by aragonite and calcite. The prevalence of calcite is favored by increased salinity in Jibou water while relative lower salinity favored prevalence of aragonite in Broscarie and Boghis waters.

The carbonated minerals are formed during the early crystallization stage due to their low solubility in water while sodium chloride crystallizes as halite in the later crystallization stages forming dendrites and well individualized crystals in Broscarie and Jibou waters and weak pellicle between carbonated branches in Boghis waters.

The physicochemical characteristics of the investigated samples and the crystallized content indicate that Boghis water is more useful for rheumatic symptoms alleviation while Jibou water is more useful for skin care benefits. Broscarie water has an equilibrate balance of salt and carbonated mineralization at moderate level indicating them as suitable for wellness and relaxation spa.

EXPERIMENTAL SECTION

Samples collection

Water samples were collected from the geothermal springs supplying system from: Broscarie spa pool in Simleul Silvaniei (measured temperature 39 °C), curing bath spa pool in Jibou (measured temperature 25 °C) and from the carbonated spring from Boghis spa (measured temperature 42 °C) in June 2025 following procedures described in standards: SR EN ISO 5667-5/2017, SR EN ISO 5667-1 /2007. Water was taken into glass recipients of 1 l hermetically closed with the gasket cap. They attend naturally the environmental temperature of about 25°C and afterwards stored in cooling case at 4 ˚C during transport to the laboratory where analyzed.

Measurement of water physicochemical properties

Physicochemical properties of the water samples were investigated according to the standard provisions: SR EN ISO 5667-3/2018 using a Hanna HI9829 multimeter measuring: pH, electrical conductivity, totals dissolved solids (TDS), and salinity. Turbidity was measured with Hanna 93703 turbidimeter with a sensitivity of 0-1000 FTU at a resolution of ± 5%. Chloride amount was measured by a Hanna HI 96711 photo-colorimeter with a resolution of 0.01 mg/l. Water total hardness was measured with Supleco MQuant test strips purchased from Sigma Aldrich, the obtained values being expressed in German degrees at a conversion rate of 1 °d= 17.8 mg/l of dissolved calcium carbonate (e.g. calcite). The measurements were effectuated in triplicate and the obtained mean values were statistically analyzed using Anova method followed by Tukey post hoc test effectuated with Origin Microcal software (Amherst, MA, USA).

Crystalline samples preparation and investigation methods

There were prepared two kind of crystallized samples: the first type was made by putting a few water drops onto glass slide to monitories the crystallization process by observation of the initial crystallization stage after 12 hours of natural drying and the final stage occurring after 24 hours. These samples reveal the crystallization process with great accuracy but cannot provide enough material for XRD investigation. The second type was made by water natural evaporation in Petri dishes followed by slow and progressive crystallization during long time (about 7 days). The crystalline formations were investigated by reflected light microscopy and mineral optical microscopy and afterward erased from the Petri dishes resulting in a white- yellow powders' which were subjected to XRD and SEM investigations.

Reflected light microscopy was effectuated using a Ulefone uSmart C01 microscope equipped with an integrated computer aided image acquiring system working on the Windows platform using png high resolution output format 720 x 1080 pixels.

Mineralogical optical microscopy (MOM) was effectuated using cross polarized light imaging performed on a Laboval 2 microscope (Carl Zeiss, Oberkochen, Germany). The images were digitally acquired through a Samsung digital system having a resolution of 10 MPx (Samsung, Hangul, Republic of Korea).

X ray diffraction (XRD) was performed with a Bruker D8 Advance diffractometer with Cu kα monochromatic radiation having a wavelength of 1.540562 Å. The patterns were registered at a speed of 1°/min. in the range of 10 – 80°. Crystal phase identification was made upon the XRD peaks using Match 1.0 software (Crystal Impact Company, Bonn, Germany).

Scanning Electron Microscopy (SEM) was done with Hitachi SU8230 operated in high vacuum mode at an acceleration voltage of 30 kV. The samples were coated with a thin layer of Pt to ensure a proper electrical conductivity. The elemental analysis was effectuated with the Energy Dispersive Spectroscopy (EDS) detector X-Max 1160 EDX (Oxford Instruments, Oxford, UK). The Pt component was subtracted from the EDS results.

REFERENCES

1. X. Shi, X. Bai, Z. Sun, J. Liu, H. Ye, L. Pang, G. Chen, H. Yan, *Geothermics*, **2025**, 131, 103402. https://doi.org/10.1016/j.geothermics.2025.103402
2. Y. Zheng, D. Nan, Z. Liu, C. Pubu, M. Zhu, H. Zhao, Y. Xing, S. Han, Q. Zeng, L. Zhang, *Geothermics*, **2025**, 131, 103374. https://doi.org/10.1016/j.geothermics.2025.103374

3. L. Yuan, P. Shen, J. Zhang, J. Yang, X. Kong, *Geothermics*, **2025**, 128, 103273. https://doi.org/10.1016/j.geothermics.2025.103273
4. Y. Jia, K. Li, L. Du, C. Zhu, F. Gao, L. Cui, Y. Shen, H. Fu, *Water,* **2025**, *17*, 1677. https://doi.org/10.3390/w17111677
5. B. Li, Q. Kong, F. Liao, G. Wang, F. Liu, L. Guo, C. Liu, Z. Shi, *Geothermics*, **2024**, 119, 102931. https://doi.org/10.1016/j.geothermics.2024.102931
6. S.E. Avram, L. Rus, V. Micle, S.S. Hola, *Water*, **2022**, 14(15), 2366. https://doi.org/10.3390/w14152366
7. L. Rus, S.E. Avram, V. Micle, *Studia UBB Chemia*, **2020**, 65(2), 257. DOI:10.24193/subbchem.2020.2.21
8. C. Krézsek, A.W. Bally, *Marine and Petroleum Geology*, **2006**, 23(4), 405-442. https://doi.org/10.1016/j.marpetgeo.2006.03.003
9. M. Venczel, I. Sabău, V. Codrea, *Nymphaea*, **2022**, 48. 77-108.
10. V. Codrea, A. Hosu, The Paleocene-Eocene formations and the Eocene/ Oligocene boundary in the Jibou area, Field Trip Guide the 4th regional meeting of IFAA, **2001**, 93-107.
11. M. Antics, M. Rosca, *Geothermics*, **2003**, 32(4-6), 361-370. https://doi.org/10.1016/S0375-6505(03)00047-6
12. M. Zhong, B. Liu, J. Chen, G. Yan, *Journal of Petroleum Science and Engineering*, **2022**, 218, 111040. https://doi.org/10.1016/j.petrol.2022.111040
13. J. Rohleder, E. Kroker, Calcium Carbonate: From the Cretaceous Period into the 21st Centruy, Springer Publishing House, **2001**.
14. H. Xue, H., J. Qian, W. Xu, *Minerals,* **2025**, *15*, 717. https://doi.org/10.3390/min15070717
15. F. Armijo, F. Maraver, M. Pozo, M.I. Carretero, O. Armijo, M.A. Fernández-Torán, M.V. Fernández-González, I. Corvillo, *Applied Clay Science*, **2016**, 126, 50-56, https://doi.org/10.1016/j.clay.2016.02.020
16. J. Walter, R. Chesnaux, V. Cloutier, D. Gaboury, *Journal of Hydrology: Regional Studies*, **2017**, 13, 168-188. https://doi.org/10.1016/j.ejrh.2017.07.004
17. T.M. Peryt, *Sedimentary Geology*, **2006**, 188–189, 379-396. https://doi.org/10.1016/j.sedgeo.2006.03.014
18. O. Gelencsér, A. Szakács, A., Gál, A. Szabo, Z. Dankházi, T. Tóth, D. Breitner, Zs. Szabó-Krausz, Cs. Szabó, Gy. Falus, *Acta Geod Geophys*, **2024**, 59, 343–365. https://doi.org/10.1007/s40328-024-00436-z
19. R.Yuan, W. Zhang, H.Gan, F. Liu, S. Wei, L. Liu, Water 2022, 14, 2235. https://doi.org/10.3390/w14142235
20. S.E. Avram, D.V. Platon, L.B. Tudoran, G. Borodi, I. Petean, *Appl. Sci.*, **2024**, 14, 10806. https://doi.org/10.3390/app142310806
21. X. Zhu, P. Chang, J. Zhang, Y. Wang, S. Li, X. Lu, R. Wang, C-Q. Liu, H.H. Teng, *Geochimica et Cosmochimica Acta*, **2022**, 339, 70-79. https://doi.org/10.1016/j.gca.2022.10.039
22. I. Petean, G. Arghir, R.F. Câmpean, M. Bărăian, A.G. Hosu Prack, *Acta Technica Napocensis Series: Matematica Aplicata si Mecanica*, **2011**, 54, 2011,193 – 200.
23. S.E. Avram, B.V. Birle, L.B. Tudoran, G. Borodi, I. Petean, *Water*, **2024**, 16, 1027. https://doi.org/10.3390/w16071027

24. S.E. Avram, B.V. Birle, C. Cosma, L.B. Tudoran, M. Moldovan, S.Cuc, G. Borodi, I. Petean, *Materials*, **2025**, 18, 1715. https://doi.org/10.3390/ma18081715
25. M. Li, X. Wang, J. You, Y. Wang, M. Zhao, P. Sun, J. Fu, Y. Yu, K. Mao, *Sustainability* **2025**, 17, 5988. https://doi.org/10.3390/su17135988
26. S. Paskucza, R. Carpa, A. Remizovschi, T. Rusu, *Scientific Papers. Series E. Land Reclamation, Earth Observation & Surveying, Environmental Engineering*, **2018**, 7, 240-246.
27. A.P. Verhagen, S.M. Bierma-Zeinstra, M. Boers, J.R. Cardoso, J. Lambeck, R. de Bie, H.C. de Vet, *Cochrane Database Syst Rev.*, **2015**, 11 (4), CD000518. https://doi.org/10.1002/14651858.CD000518.pub2
28. H. Romay-Barrero,J. Herrero-López, J.A. Llorente-González, G. MelgarDel Corral, R. Palomo-Carrión, I. Martínez-Galán, *Balneo and PRM Research Journal*, **2022**, 13(4): 527. https://doi.org/10.12680/balneo.2022.527
29. A. Huang, S. Seité, T. Adar, *Clinics in Dermatology*, **2018**, 36, 363-368. https://doi.org/10.1016/j.clindermatol.2018.03.010
30. V. Milanković, J. Djuriš, A. Tubić, J. Agbaba, S. Forkapić, M. Lukić, *RSC Advances*, **2025**, 15, 17755-17775. https://doi.org/10.1039/d5ra01252j
31. K. Wątor, *Water Resources and Industry*, **2024**, 31, 100248. https://doi.org/10.1016/j.wri.2024.100248
32. M.V. Fernández-González, M.I. Carretero, J.M. Martín-García, A. Molinero-García, R. Delgado, *Applied Clay Science*, **2021**, 202, 105969. https://doi.org/10.1016/j.clay.2020.105969
33. T. Barhoumi, I. Bekri-Abbes, E. Srasra, *Comptes Rendus Chimie*, **2019**, 22, 126-131. https://doi.org/10.1016/j.crci.2018.11.006
34. G. Gerencsér, E. Murányi, K. Szendi, C. Varga, *Applied Clay Science*, **2010**, 50, 47-50. https://doi.org/10.1016/j.clay.2010.06.022
35. M.T. Baschini, G.R. Pettinari, J.M. Vallés, C. Aguzzi, P. Cerezo, A. López-Galindo, M. Setti, C. Viseras, *Applied Clay Science*, **2010**, 49, 205-212. https://doi.org/10.1016/j.clay.2010.05.008